Chemical Science

ROYAL SOCIETY OF CHEMISTRY

EDGE ARTICLE

View Article Online
View Journal

Check for updates

Cite this: DOI: 10.1039/d6sc01178k

All publication charges for this article have been paid for by the Royal Society of Chemistry

Individually addressable multichannel nanoelectrodes reveal spatially resolved functional heterogeneity of vesicles in single cells

Chuchu Xu,†[a] Ruolin Liu,†[ac] Yuhao Zheng,[a] Yue Chen,[a] Irina Svir,[b] Alexander Oleinick,*[b] Zhongqun Tian,[ac] Christian Amatore[ab] and Keke Hu*[ac]

Nanoelectrodes are powerful tools for high-resolution electrochemical measurements, yet a long-standing limitation has been the inability to perform simultaneous, spatially resolved measurements across multiple domains within a single confined system. Here we develop an individually addressable multichannel nanoelectrode platform that preserves nanoscale spatial resolution while enabling independent and parallel electrochemical recording. The platform supports batch fabrication of nanoelectrodes with either hollow or filled architectures, providing precise geometric control for applications ranging from confined intracellular environments to open electrochemical interfaces, as validated by electron microscopy, voltammetry, and simulations. Applied to single living cells, hollow multichannel electrodes enable minimally disruptive, region-resolved intracellular recording from nuclear-adjacent and membrane-proximal domains, providing direct quantitative evidence for functional heterogeneity of vesicle populations. These findings uncover a previously inaccessible mechanistic link between subcellular vesicle organization and secretion efficiency, with direct implications for how neuroendocrine and neuronal cells achieve rapid yet regulated chemical signaling.

Received 10th February 2026
Accepted 1st April 2026

DOI: 10.1039/d6sc01178k

rsc.li/chemical-science

Open Access Article. Published on 10 April 2026. Downloaded on 5/1/2026 4:20:06 AM.
This article is licensed under a Creative Commons Attribution-NonCommercial 3.0 Unported Licence.

Introduction

Nanoelectrodes have emerged as powerful tools for probing chemical processes with nanoscale spatial resolution, enabling electrochemical measurements in confined environments ranging from single cells to heterogeneous interfaces. Single-channel nanoelectrodes—including carbon fiber nanotips, nanowires, nanopipettes, and nanopores—have enabled chemically specific detection of intracellular messengers, reactive species, and redox-active metabolites, providing unique insight into cellular signaling and chemical communication.[1–6] As probes in Scanning Electrochemical Microscopy (SECM) and Scanning Electrochemical Cell Microscopy (SECCM), nanoelectrodes have also enabled nanoscale interrogation of interfacial electron transfer and catalytic activity.[7–9] In addition, double- and four-barrel nanopipette-based nanoelectrodes integrating electrochemical sensing with complementary techniques—such as SECCM–SECM, or electrochemical-mass spectrometry—have expanded nanosensor capabilities.[10–12] However, despite these advances, existing nanoelectrode platforms remain intrinsically limited to single detection sites or point-by-point scanning, preventing simultaneous interrogation of spatially heterogeneous chemical processes.

In neuroendocrine and neuronal systems, chemical communication is mediated by the regulated release of signaling molecules from nanoscale secretory vesicles. These vesicles are not uniformly distributed within cells but exhibit pronounced spatial organization, with vesicle populations enriched near the plasma membrane and depleted toward the cell interior. This spatial arrangement underlies functional heterogeneity among vesicle subpopulations and is believed to play a critical role in regulating secretion efficiency, signaling dynamics, and stimulus–response coupling in secretory cells.[13] Understanding how vesicle organization within subcellular domains influences chemical release is therefore essential for elucidating the mechanisms of neuroendocrine communication and its dysregulation in disease. Ultrastructural electron microscopy has revealed the uneven vesicle distributions in fixed cells, while optical imaging and electrophysiological measurements have provided insight into vesicle fusion dynamics and calcium dependence.[14–17] However, these approaches primarily report membrane-associated events and lack direct chemical specificity, preventing quantitative

[a]State Key Laboratory of Physical Chemistry of Solid Surfaces, College of Chemistry and Chemical Engineering, Xiamen University, Xiamen 361005, China
[b]Chimie Physique et Chimie du Vivant, Département de Chimie, École Normale Supérieure PSL University, Sorbonne Université, CNRS, 24 rue Lhomond, 75005 Paris, France
[c]Discipline of Intelligent Instrument and Equipment, Xiamen University, Xiamen 361005, China
† Equal contribution.

© 2026 The Author(s). Published by the Royal Society of Chemistry

Open Access Article. Published on 10 April 2026. Downloaded on 5/1/2026 4:20:06 AM. This article is licensed under a Creative Commons Attribution-NonCommercial 3.0 Unported Licence.

correlation between vesicle localization, molecular content, and release kinetics. Intracellular vesicle impact electrochemical cytometry (IVIEC) offers chemically specific, millisecond-resolved quantification of single-vesicle release.[1,18] In this approach, carbon nanopipette electrodes (CNPs) provide a confined nanoelectrochemical environment in which vesicles entering the nanochannel undergo rupture and oxidation of their molecular contents, producing characteristic amperometric spikes that report vesicle content and release kinetics.[19,20] However, IVIEC typically relies on single-channel nanoelectrodes and therefore cannot resolve the spatial heterogeneity of vesicle pools within individual living cells. As a result, a fundamental question remains unresolved: how subcellular vesicle organization governs secretion efficiency and chemical signaling dynamics in living cells.

Here we develop an individually addressable multichannel nanoelectrode (MANE) platform that preserves nanoscale spatial resolution while enabling simultaneous, independent electrochemical recording. Applied to single chromaffin cells, hollow MANEs allow minimally perturbative intracellular insertion and parallel subcellular measurements, revealing pronounced differences in vesicle density, chemical content, and release kinetics between nuclear-adjacent and membrane-proximal domains. These results establish a direct mechanistic link between subcellular vesicle organization and secretion efficiency, addressing a central challenge in understanding neuronal and neuroendocrine chemical communication.

Experimental

Fabrication of multichannel carbon nanopipette electrodes

Multichannel carbon nanopipette electrodes were fabricated from multibarrel quartz capillaries (four-barrel unless otherwise specified) using a laser-based micropipette puller. Pulling parameters were optimized to achieve nanoscale tip diameters while maintaining mechanical robustness across all channels. The pulled multichannel pipettes were subsequently subjected to chemical vapor deposition (CVD) for carbon growth inside each nanochannel.

Methane was used as the carbon precursor with argon as the inert protective gas. By adjusting the CVD temperature, gas flow rate, and deposition time, two distinct electrode configurations were obtained: hollow multichannel carbon nanopipettes with nanoscale orifices and filled multichannel electrodes with disk-like carbon surfaces at the tip. Hollow configurations were used for intracellular and vesicle measurements, whereas filled configurations were employed for diffusion-controlled interfacial electrochemical characterization. Detailed fabrication parameters and optimization procedures are provided in the SI.

Electrochemical characterization in standard solution

Electrochemical measurements in standard redox solutions were performed using potentiostats, with channels either individually addressed or electrically connected as a combined working electrode. CV was carried out in 1 mM FcMeOH prepared in 100 mM KCl. A Ag/AgCl electrode was used as the reference and counter electrode.

For independent channel characterization, each channel of a multichannel nanoelectrode was connected individually to a separate potentiostat. For additive-throughput measurements, multiple channels were jointly connected to a single working electrode input. Inter-channel electrical isolation was evaluated by measuring resistance between adjacent channels using a dual-probe configuration.

Structural and electrochemical validation of multichannel nanoelectrodes

The geometry and structural integrity of the multichannel nanoelectrodes were characterized by scanning electron microscopy (SEM), which was used to determine single-channel orifice dimensions, overall tip diameter, and channel symmetry. Electrochemical behavior was evaluated by cyclic voltammetry in FcMeOH solutions to assess channel-to-channel uniformity, thin-layer *versus* diffusion-controlled response, and additive current behavior when multiple channels were operated simultaneously. For filled-type electrodes, effective single-channel radii were estimated from steady-state limiting currents using the nanodisk relation $i_l = 4xnFDca$ and compared with SEM-derived dimensions. Finite-element simulations were used to further validate diffusion behavior and current scaling in single- and multichannel configurations (see SI).

Vesicle preparation and vesicle impact electrochemical cytometry

Chromaffin vesicles were isolated from bovine adrenal medulla following established protocols with minor modifications. Isolated vesicles were suspended in phosphate-buffered saline (PBS) and diluted to the desired concentration immediately prior to measurements.

Vesicle impact electrochemical cytometry (VIEC) experiments were conducted by immersing the hollow multichannel nanoelectrode into the vesicle suspension and applying a constant oxidation potential. Vesicle rupture events were recorded as amperometric spikes and analyzed to extract the number of molecules released per vesicle and kinetic parameters, including event half-widths. Additional details of vesicle isolation and data analysis are provided in the SI.

Cell culture and intracellular measurements

Primary bovine chromaffin cells were cultured on standard cell culture dishes under standard conditions. For intracellular measurements, cells were transferred to a isotonic buffer prior to experiments.

Four-channel hollow carbon nanopipettes were inserted into single living chromaffin cells using a micromanipulator under combined optical and electrochemical guidance. The nucleus was fluorescently labeled to facilitate control of insertion depth and positioning. Because chromaffin cell nuclei are typically off-center, electrodes were introduced from the side nearest the nucleus, enabling two channels to approach the perinuclear

© 2026 The Author(s). Published by the Royal Society of Chemistry

Open Access Article. Published on 10 April 2026. Downloaded on 5/1/2026 4:20:06 AM. This article is licensed under a Creative Commons Attribution-NonCommercial 3.0 Unported Licence.

region while the remaining two channels were positioned near the plasma membrane.

Insertion depth was monitored by real-time current feedback and fluorescence imaging. Repeated trials established an optimal insertion depth slightly above the nuclear membrane, approximately 2–3 μm below the cell surface, which enabled reliable dual-site intracellular recording with minimal perturbation. Cell viability after electrode insertion was assessed by bright-field imaging and fluorescence-based assays (see SI).

Parallel subcellular amperometric recording

For parallel subcellular recordings, two channels positioned near the plasma membrane were connected to one headstage, while the two perinuclear channels were connected to a second headstage, allowing simultaneous amperometric measurements from two distinct intracellular regions within the same cell. Control experiments were performed by reversing channel-to-headstage connections to exclude channel-specific or wiring-related artifacts.

Amperometric data were analyzed to quantify vesicle event frequency, molecular content ($N_{molecules}$), and release kinetics.

Statistical analysis

All quantitative data are reported as mean ± standard deviation (SD) unless otherwise noted. Statistical significance was assessed using two-sample (unpaired) Student's *t*-tests as specified in the figure legends. A p value < 0.05 was considered statistically significant. No data points were excluded unless explicitly stated.

Results and discussion

Design and fabrication of individually addressable multichannel nanoelectrodes

As illustrated in Fig. 1A, multibarrel quartz capillaries were first heat-pulled into nanoscale pipettes and subsequently subjected to methane pyrolysis under controlled chemical vapor deposition (CVD) conditions, conceptually similar to single-channel methods but requiring precise pulling and deposition control to maintain channel uniformity and separation.[21,22] Depending on the deposition time, temperature, and methane/argon flow rate, either open carbon nanopipettes (open CNPs) or completely filled multichannel carbon electrodes were obtained, enabling electrochemical architectures tailored for confined intracellular or open interfacial environments. The open-type electrodes feature hollow carbon channels with exposed interiors, whereas the filled-type electrodes can be polished to obtain flat carbon surfaces suitable for planar electrochemical applications such as SECM. This fabrication strategy enables precise control and batch fabrication of nanoelectrodes with tunable channel number, orifice size (down to ~20 nm in diameter per channel, Fig. S1), taper angle, and internal configuration. Representative SEM images

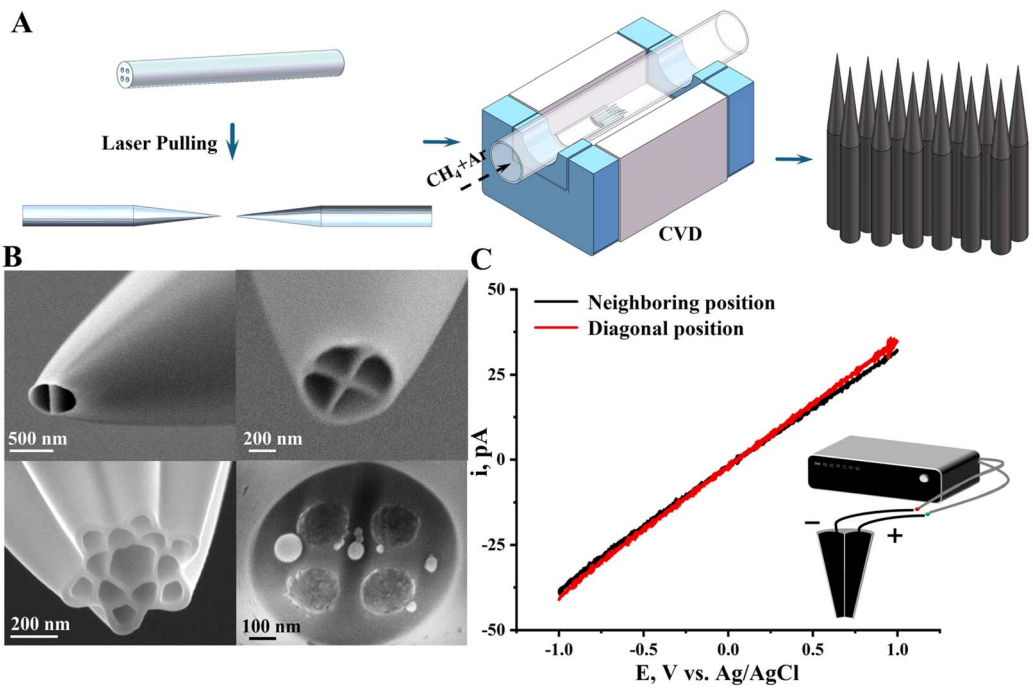

Fig. 1 Fabrication and structural characterization of individually addressable multichannel nanoelectrodes (MANEs). (A) Schematic illustration of the fabrication process for individually addressable MANEs, including multibarrel quartz capillary pulling and carbon deposition through CVD. (B) SEM images of two-, four-, and thirteen-channel hollow-type MANEs (overall diameter of 560, 620, 640 nm) and a four-channel filled-type MANE (overall diameter of 690 nm) showing well-defined, spatially separated carbon nanochannels at the tip. (C) Dual-probe resistance measurement on a four-channel MANE using a model circuit to assess inter-channel insulation ($v = 50$ mV s^{-1}, the resistance value (>10^{13} Ω) was obtained from the slope of the corresponding I–V curves).

Open Access Article. Published on 10 April 2026. Downloaded on 5/1/2026 4:20:06 AM. This article is licensed under a Creative Commons Attribution-NonCommercial 3.0 Unported Licence.

(Fig. 1B) show hollow MANEs with 2, 4, and 13 channels and filled 4-channel MANEs, all exhibiting uniform geometry among channels within each electrode, even for high-multiplicity designs. Dual-probe measurements on four-channel MANEs (Fig. 1C) yielded inter-channel resistance values above 10^{13} Ω, confirming excellent insulation and electrical independence among channels.

Thin-layer electrochemical behavior and independent operation of hollow multichannel nanoelectrodes

Cyclic voltammetry was first performed individually yet simultaneously at each channel of a hollow four-channel nanoelectrode using 1 mM ferrocenemethanol (FcMeOH) in 100 mM KCl (Fig. 2A). All four channels exhibited nearly identical, peak-shaped voltammograms with steady-state currents of ~20 pA and comparable peak currents, indicating uniform orifice sizes, similar electroactive surface areas, and minimal crosstalk across the independent channels. The peak-shaped profiles arise from thin-layer-like electrolysis occurring within the confined nanoscale cavities.[23] Notably, the peak current gradually increased over successive scans, consistent with progressive infiltration of the electrolyte into the hollow channels and enlargement of the effective electroactive volume.[24] When all four channels of the hollow MANEs were simultaneously connected to a single working-electrode input (Fig. 2B), the resulting CVs displayed increased total current and steady-state current (~77 pA) while maintaining a similar peak shape, with only minor shifts in peak potential—consistent with the additive contribution of four independent thin-layer domains formed at each hollow tip. The presence of well-defined peak-shaped responses across all configurations confirms that the electrochemical response is dominated by thin-layer behavior inside the nanoscale channels, while steady-state contributions from radial diffusion can be largely neglected. COMSOL simulations further confirmed that currents originating from the thin-layer domains inside each channel are additive and independent, whereas the edge-derived (radial-like) steady-state diffusion components exhibit mutual competition when the channels are operated together (see SI for details).

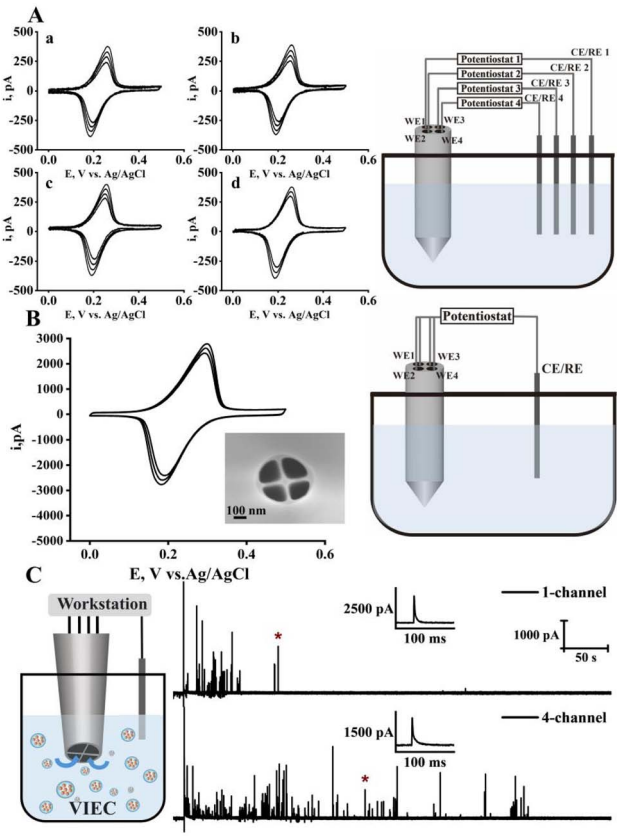

Fig. 2 Electrochemical characterization and enhanced vesicle-detection capability of four-channel hollow carbon nanoelectrodes. (A) Individual cyclic voltammograms (CVs) recorded from each of the four channels of a single open CNPs (single orifice diameter, ~140 nm) in 1 mM FcMeOH with 100 mM KCl. (Right) schematic of the configuration for independent yet simultaneous channel measurements. (B) CVs recorded from the same open CNP with all four channels connected simultaneously to a single working-electrode input, with the corresponding schematic shown at right. (Inset) SEM image of the tip showing four hollow carbon channels with nanoscale spacing. (C) Schematic illustration and representative amperometric traces of vesicle-impact electrochemical cytometry (VIEC) measurements in chromaffin-vesicle suspensions recorded using the same pair of identical four-channel electrode (SEM image in Fig. S11). Top: single-channel configuration; bottom: four channels connected simultaneously (58 *vs.* 178 rupture events).

Enhanced vesicle detection efficiency through parallelized hollow multichannel nanoelectrodes

The four-channel open CNP was further applied to VIEC measurements in chromaffin vesicle suspensions to demonstrate its capability for high-efficiency vesicle detection (Fig. 2C).[19] Two representative current traces were recorded from the same pair of identical four-channel electrode (SEM image in Fig. S11): one with only a single channel active and another with all four channels connected. The four-channel configuration resulted in a substantially higher number of vesicle rupture events—approximately three times more than the single-channel trace, reflecting the expected statistical enhancement from multiple active detection zones. This capability is particularly critical under low vesicle density conditions. The increase was not strictly four-fold because simultaneously active channels compete diffusionally for vesicles in the shared suspension. These results demonstrate that the hollow multichannel architecture—with nanoscale orifices and an enlarged effective surface area—enables high sensitivity and independent operation, offering additive throughput and flexible configuration for multisite electrochemical measurements in confined environments.

Filled multichannel nanoelectrodes enable diffusion-controlled multisite electrochemical measurements

Beyond confined biological environments, similar spatial heterogeneity exists in electrochemical systems such as catalytic surfaces and battery materials, where direct diffusion control at open interfaces is required. The filled multichannel nanoelectrode configuration provides a more suitable platform for

© 2026 The Author(s). Published by the Royal Society of Chemistry

Open Access Article. Published on 10 April 2026. Downloaded on 5/1/2026 4:20:06 AM.
This article is licensed under a Creative Commons Attribution-NonCommercial 3.0 Unported Licence.

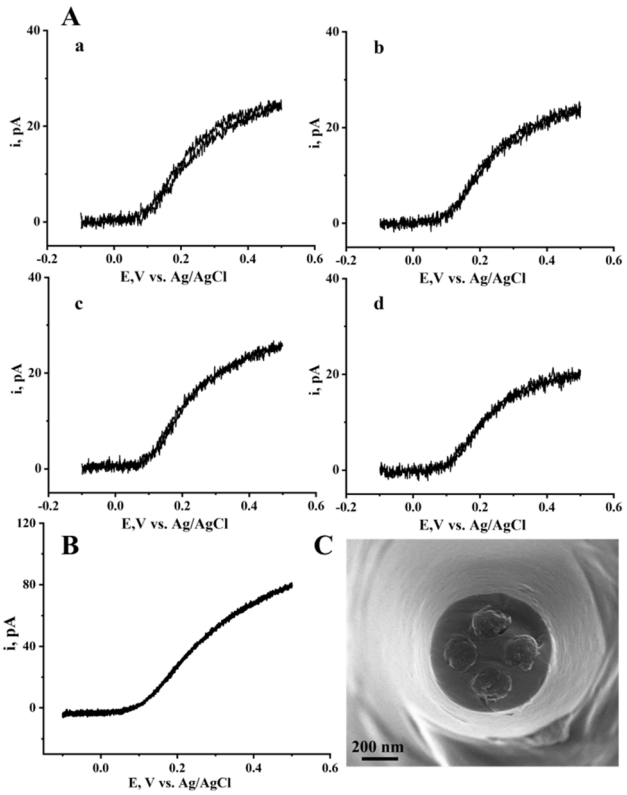

Fig. 3 Diffusion-controlled electrochemical behavior of filled-type four-channel carbon nanopipette electrodes. (A) Individual CVs recorded from each of the four channels of a filled-type carbon nanopipette electrode (1 mM FcMeOH, 100 mM KCl). (B) CV obtained when all four channels of the same electrode were connected simultaneously to a single working-electrode input. (C) The corresponding SEM image showing disk-shaped carbon surfaces at the tip.

high-resolution mapping of spatially heterogeneous electrochemical processes. Unlike the hollow configuration, the filled-type design ensures direct electrical contact with the external solution, thereby producing classical steady-state diffusion behavior. As shown in Fig. 3A, individually recorded CVs from each of the four channels in 1 mM FcMeOH solution exhibited well-defined sigmoidal shapes with comparable limiting currents (24.4, 25.5, 25.5, and 20.3 pA), reflecting generally uniform channel geometry and diffusion characteristics. When the four channels were connected to a single working electrode input (Fig. 3B), the resulting CV remained sigmoidal but showed a slightly lower limiting current (84.6 pA) than the sum of individual channels (94.7 pA), which can be attributed to the formation of competing diffusion layers at adjacent disks resulting in decrease of available solution to each disk and overall lower individual currents. The corresponding SEM image (Fig. 3C) confirms the formation of disk-like carbon surface (single-channel radius of 93, 106, 99, 86 nm; overall outer diameter 678 nm) at the tip. The single-channel radius estimated from the steady-state current using the nanodisk relation ($i_l = 4xnFDca$[23]) gives values close to those derived from SEM, which supports its applicability for multi-channel radius estimation. Additional COMSOL simulations validating the diffusion behavior of single and multiple disks are provided in the SI (Fig. S8–S10). This disk-array configuration complements the hollow type by providing stable and reproducible interfaces for surface-sensitive electrochemical studies.

Parallel subcellular electrochemical mapping of vesicle pools in single living cells

We next applied four-channel open CNPs (overall diameter ~800 nm, channel diameter ~300 nm, quartz walls ~60 nm, center-to-center spacing ~400 nm, SEM image in Fig. S13) to probe vesicle-pool heterogeneity within single chromaffin cells—neuroendocrine cells in the adrenal medulla that release catecholamines and other signaling molecules *via* exocytosis. In this configuration, two channels near the plasma membrane were connected to headstage 1 and two near the perinuclear region to headstage 2 (Fig. 4A), enabling simultaneous amperometric recordings from two intracellular regions of the same cell. Electrode insertion was guided by fluorescence and current feedback: nuclear-targeted staining (Fig. 4B, left) located the nucleus, and live-cell bright-field imaging (Fig. 4B, right) visualized real-time insertion. As the nucleus in chromaffin cells is typically off-center, the electrode was introduced from the side nearest the nucleus, ensuring that two channels were positioned near the perinuclear region and two near the plasma membrane. Repeated trials determined the optimal insertion depth to be just above the nuclear membrane—typically 2–3 μm below the cell surface—ensuring minimal perturbation (see SI for manipulation details and cell viability tests) and reliable dual-site recordings within the cytoplasmic region. Furthermore, owing to the hollow nanochannel configuration, intracellular measurements only require insertion of the very end of the electrode tip. Representative amperometric traces recorded simultaneously from the two regions are shown in Fig. 4C. The membrane-proximal region exhibited a markedly higher frequency of vesicle rupture events than the perinuclear region (average 348 *vs.* 18 events per cell), indicating a pronounced enrichment of releasable vesicles near the plasma membrane. This ~20-fold difference in event frequency provides direct quantitative evidence for strong spatial heterogeneity in vesicle density within a single cell. Quantitative analysis further revealed that vesicles located in the perinuclear region released significantly larger numbers of molecules per event ($N_{molecules}$) and exhibited longer event half-widths ($t_{1/2}$) compared to membrane-proximal vesicles (Fig. 4D). In contrast, vesicles near the plasma membrane contained fewer chemical messengers and released them more rapidly, indicating functionally distinct vesicle subpopulations defined by subcellular location. Although some diffusional overlap between the two regions is unavoidable, its contribution appears minor compared with the strong local preference observed experimentally. This spatial organization is consistent with the commonly proposed model in which membrane-proximal vesicles preferentially contribute to rapid secretion, while more internal vesicles may serve as a reserve population that can be recruited during sustained signaling. Such spatial regulation may therefore provide a structural basis for achieving rapid yet finely tuned chemical communication in neuroendocrine and neuronal systems.

Open Access Article. Published on 10 April 2026. Downloaded on 5/1/2026 4:20:06 AM.
This article is licensed under a Creative Commons Attribution-NonCommercial 3.0 Unported Licence.

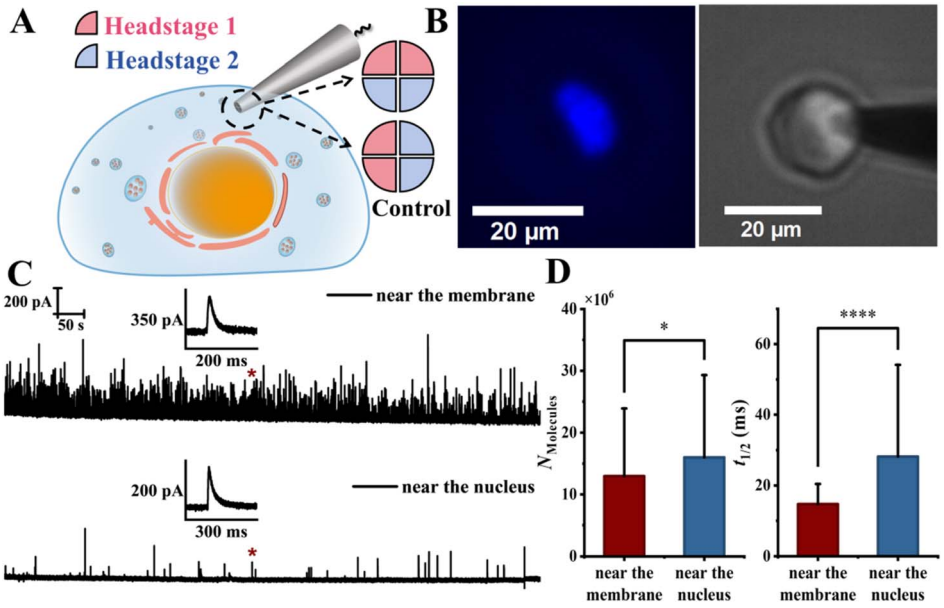

Fig. 4 Parallel subcellular amperometric recording using four-channel hollow carbon nanoelectrodes reveals spatial heterogeneity of vesicle release within single chromaffin cells. (A) Schematic illustration of a four-channel open CNP for dual-site amperometric recordings within a single chromaffin cell. Two upper channels positioned near the plasma membrane (pink, headstage 1) and two lower channels near the perinuclear region (blue, headstage 2) enable simultaneous monitoring of distinct subcellular domains; an alternative channel-to-headstage connection was used as a control configuration and these control experiments were performed in different cells (as illustrated in Fig. 5). (B) Fluorescence image (left) showing nuclear staining for nucleus localization and confirmation of subcellular electrode positioning, and corresponding bright-field live-cell image (right) during electrode insertion. (C) Representative amperometric traces recorded simultaneously from the subplasmalemmal (top) and perinuclear (bottom) regions of the same cell. (D) Statistical comparison of vesicular content ($N_{molecules}$) and event half-widths ($t_{1/2}$) between the two regions showed significant differences (data from 6 cells; 2086 *vs.* 108 events; $p < 0.05$ and $p < 0.001$ for $N_{molecules}$ and $t_{1/2}$, respectively; two-sample unpaired Student's *t*-test; distributions are shown in Fig. S16; error bars represent standard deviation).

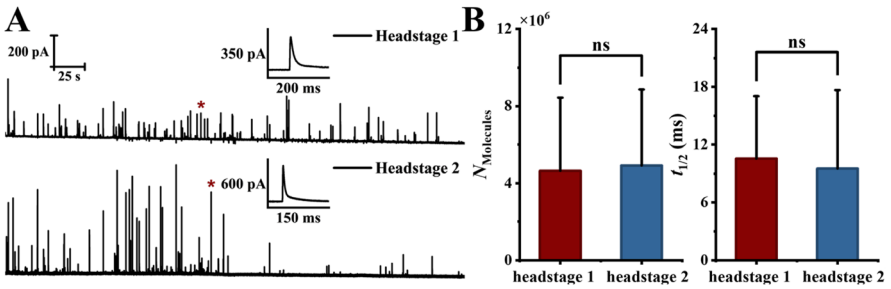

Fig. 5 Control experiment validating that the spatial differences observed in Fig. 4 are not due to channel- or wiring-related artifacts. (A) Representative simultaneous amperometric traces recorded from two headstages under the control configuration, where the channel-to-headstage connections were reversed relative to the main experiment (schematic in Fig. 4A). (B) Statistical comparison of $N_{molecules}$ and $t_{1/2}$ between the two headstages under this reversed configuration, showing no significant difference (data from 8 cells; 235 *vs.* 208 events; distributions are shown in Fig. S17; $p > 0.05$ (two-sample *t*-test); error bars represent standard deviation).

Control experiments exclude channel- and wiring-related artifacts

To exclude channel-specific variability or asymmetry in electrical wiring, a control configuration was tested (Fig. 5) with left and right channels assigned to headstages 1 and 2 (as illustrated in Fig. 4A). No significant differences in event frequency, $N_{molecules}$ or $t_{1/2}$ were observed (Fig. 5A and B), confirming that the observed spatial differences shown in Fig. 4 arise from genuine subcellular heterogeneity.

Conclusions

The ability to perform parallel, region-resolved electrochemical measurements within a single living cell provides direct access to the spatial organization of vesicle-mediated secretion. By simultaneously probing membrane-proximal and perinuclear regions, we uncover pronounced functional heterogeneity of vesicle pools that is inaccessible to single-point or scanning-based techniques. The markedly higher vesicle density near

© 2026 The Author(s). Published by the Royal Society of Chemistry

Open Access Article. Published on 10 April 2026. Downloaded on 5/1/2026 4:20:06 AM.
This article is licensed under a Creative Commons Attribution-NonCommercial 3.0 Unported Licence.

the plasma membrane, together with reduced molecular content and faster release kinetics, indicates that membrane-proximal vesicles are optimized for rapid, stimulus-evoked secretion. In contrast, perinuclear vesicles exhibit larger chemical content and slower release dynamics, consistent with a reserve pool supporting sustained secretion. This organization establishes a direct mechanistic link between subcellular vesicle localization and secretion efficiency, providing a plausible strategy for achieving rapid yet precisely tuned chemical signaling in neuroendocrine and neuronal systems. Future studies will apply this platform to investigate how vesicle release dynamics evolve under physiological stimulation and to explore the molecular mechanisms that regulate spatial vesicle heterogeneity, including vesicle transport, docking processes, and cytoskeletal organization. Moreover, this platform can be readily extended to other cell types that release electroactive signaling molecules.

Beyond the biological insight, the multichannel nanoelectrode platform itself represents a fundamental advance in nanoelectrochemical measurement science. By integrating nanoscale spatial resolution with simultaneous, independently addressable recording sites, it overcomes intrinsic limitations of conventional single-channel nanoelectrodes and scanning methods. The tunable hollow and filled configurations further extend applicability from confined intracellular environments to open interfacial systems. Together, this work establishes a general framework for multisite, spatially resolved electrochemical analysis, enabling quantitative studies of vesicle-mediated signaling in neuronal, neuroendocrine, and pancreatic islet systems, while naturally extending to spatially heterogeneous electrochemical processes at open interfaces.

Author contributions

K. H. conceived and supervised the project. C. X. and R. L. performed nanoelectrode fabrication, electrochemical characterization, vesicle cytometry, and intracellular experiments. Y. Z. and Y. C. assisted with cell experiments and data analysis. A. O. and I. S. contributed to theoretical analysis and electrochemical modeling. Z.-Q. T. and C. A. provided scientific discussion and guidance. K. H. and A. O. wrote the manuscript with input from all authors.

Conflicts of interest

There are no conflicts to declare.

Data availability

The data that support the findings of this study are available within the article and its supplementary information (SI). Additional data are available from the corresponding author upon reasonable request. Supplementary information: experimental details, electrode fabrication and characterization, electrochemical modeling and simulations, validation of minimally invasive intracellular measurements, and supplementary data supporting spatially resolved vesicle heterogeneity in single cells. See DOI: https://doi.org/10.1039/d6sc01178k.

Acknowledgements

We gratefully acknowledge Xiamen Xiashang Huangjinxiang Food Co., Ltd, Jimei Meat Processing Plant for providing bovine adrenal glands. This work was supported by the National Natural Science Foundation of China (General Program Grant No. 22574135 and Youth Program Grant No. 22204133) and the Fujian Provincial Natural Science Foundation Outstanding Youth Fund (Grant No. 2024J09007). In Paris this work was supported in part by CNRS, Ecole Normale Superieure, PSL University, and Sorbonne University (UMR 8228 CPCV). We also acknowledge the Sino-French IRP CNRS NanoBioCatEchem for its support. CA thanks Xiamen University for his Distinguished Visiting Professor position.

References

1 X. Li, S. Majdi, J. Dunevall, H. Fathali and A. G. Ewing, *Angew. Chem., Int. Ed.*, 2015, **54**, 11978.
2 Y.-L. Ying, *et al.*, *J. Am. Chem. Soc.*, 2018, **140**, 5385.
3 Y. T. Li, *et al.*, *Angew. Chem., Int. Ed.*, 2014, **53**, 12456.
4 R. Pan, D. Wang, K. Liu, H.-Y. Chen and D. Jiang, *J. Am. Chem. Soc.*, 2022, **144**, 17558.
5 P. Actis, *et al.*, *ACS Nano*, 2014, **8**, 875.
6 K. Hu, Y. Li, S. A. Rotenberg, C. Amatore and M. V. Mirkin, *J. Am. Chem. Soc.*, 2019, **141**, 4564.
7 T. Sun, *et al.*, *Proc. Natl. Acad. Sci. U. S. A*, 2019, **116**, 11618.
8 K. Barman, X. Wang, R. Jia and M. V. Mirkin, *J. Am. Chem. Soc.*, 2021, **143**, 8547.
9 N. Ebejer, *et al.*, *Annu. Rev. Anal. Chem.*, 2013, **6**, 329.
10 Y. Takahashi, *et al.*, *Angew. Chem., Int. Ed.*, 2011, **50**, 9638.
11 C. Gu, *et al.*, *J. Am. Chem. Soc.*, 2019, **141**, 13212.
12 B. Paulose Nadappuram, *et al.*, *Anal. Chem.*, 2015, **87**, 3566.
13 E. Neher, *Neuron*, 1998, **20**, 389.
14 L. M. Koval, E. N. Yavorskaya and E. A. Lukyanetz, *Gen. Comp. Endocrinol.*, 2001, **121**, 261.
15 H. Park, Y. Li and R. W. Tsien, *Science*, 2012, **335**, 1362.
16 E. Neher and A. Marty, *Proc. Natl. Acad. Sci. U. S. A*, 1982, **79**, 6712.
17 R. Heidelberger, C. Heinemann, E. Neher and G. Matthews, *Nature*, 1994, **371**, 513.
18 N. T. N. Phan, X. Li and A. G. Ewing, *Nat. Rev. Chem.*, 2017, **1**, 0048.
19 K. Hu, *et al.*, *J. Am. Chem. Soc.*, 2020, **142**, 16910.
20 K. Hu, K. L. Le Vo, A. Hatamie and A. G. Ewing, *Angew. Chem., Int. Ed.*, 2022, **61**, e202113406.
21 R. Singhal, *et al.*, *Nanotechnology*, 2010, **21**, 015304.
22 K. Hu, *et al.*, *J. Solid State Electrochem.*, 2013, **17**, 2971.
23 Y. Yu, *et al.*, *Anal. Chem.*, 2014, **86**, 3365.
24 G. Laucirica, G. A. Crespo and M. Cuartero, *Anal. Chem.*, 2025, **97**, 17659.